# Application of a Cryo-FIB-SEM-$\mu$Raman Instrument to Probe the Depth of Vitreous Ice in a Frozen Sample

Mouad Essani, Jean-Yves Mevellec, Baptiste Charbonnier, Philippe Moreau, Hilel Moussi, Pierre Weiss, Jean Le Bideau, Maxime Bayle, Bernard Humbert, Patricia Abellan

# Application of cryo FIB-SEM-µRaman instrument to probe the depth of vitreous ice in a frozen sample

Mouad Essani[1*], Jean-Yves Mevellec[1], Baptiste Charbonnier[2], Philippe Moreau[1], Hilel Moussi[1,2], Pierre Weiss[3], Jean Le Bideau[1], Maxime Bayle[1], Bernard Humbert[1], Patricia Abellan[1*]

[1]Nantes Université, CNRS, Institut des Matériaux de Nantes Jean Rouxel (IMN), F-44000 Nantes, France

[2]Nantes Université, INSERM, UMR 1229 RMeS/ONIRIS, Regenerative Medicine and Skelton laboratory, F-44042 Nantes, France

[3]Nantes Université, INSERM, UMR 1229 RMeS/ONIRIS, Regenerative Medicine and skeleton laboratory, F-44042 Nantes, France

**ABSTRACT:** The development of instruments combining multiple characterization and imaging tools drove huge advances in material science, engineering, biology and other related fields. Notably, the coupling of SEM with micro-Raman spectrometry (µRaman) provides means for the correlation between structural and physicochemical properties at surfaces, while dual focused ion beam (FIB)-scanning electron microscopes (SEMs) operating under cryogenic conditions (cryo FIB-SEM) allows for the analysis of the ultrastructure of materials *in situ* and in their native environment. In cryo FIB-SEM, rapid and efficient methods for assessing vitrification conditions *in situ* are required for accurate investigation of the original structure of hydrated samples. This work reports for the first time the use of cryo FIB-SEM-µRaman instrument to efficiently assess the accuracy of cryo-fixation methods. Analyses were performed on plunge-freezed highly hydrated calcium phosphate cement (CPC) and gelatin composite. By making a trench of a defined thickness with FIB, µRaman analyses were carried out at a specific depth within the frozen material. Results show that µRaman signal is sensitive to the changes in the molecular structures of the aqueous phase and can be used to examine the depth of vitreous ice in frozen samples. The method presented in this work provides a reliable way to avoid imaging artefacts in cryo FIB-SEM that are related to cryo-fixation, and can be generally applied to all vitreous samples, in life sciences, biology and material sciences, regardless of the sample preparation method (i.e. by HPF, plunge freezing, …).

In biology, life sciences, and most recently in material science, the observation with cryogenic electron microscopy (EM) of the native structure of materials interfaces, notably at solid-liquid interfaces [1,2], and defective or specific sites in materials [3,4] still presents a considerable challenge. In cryo-scanning EM (cryo-SEM), the complexity in preserving the original structure of biological and high water content materials lies in avoiding structural artefacts during the cryo-fixation/freezing processes. As these artefacts can be related to various phenomena (e.g. changes of the position of organelles [5], aggregation of soluble substances [6]) they commonly result from structural damage due to the formation of ice crystals [6,7]. Vitrification of water or aqueous solutions contained in hydrated soft materials is an essential process in structural investigations under cryogenic conditions and should ideally be achieved without the formation of organized crystalline ice.

Vitreous ice can be formed by rapidly cooling liquid water below its glass transition temperature (Tg ≈136 K). The rapid cooling rate prevents the spontaneous nucleation and growth of ice crystals, which results in a lack of long-range order in the water molecular arrangement. Different cryo-fixation techniques enabling to achieve ice vitrification in hydrated samples are now available. These include plunge freezing of samples into a cryogen (e.g. liquid nitrogen slush or liquid ethane) [8], the use of cryo-protectants (e.g. glycerol, methanol, polyvinylpyrolidone) [9] and high pressure freezing (HPF) [10]. Although, HPF is considered by far the most reliable method in both providing the largest volume of vitrified ice and minimizing cryo-fixation artefacts [6, 11], it still presents some disadvantages. Among which is the risk of contaminating the sample by the heat conductive filler and only a small amount of material can be frozen which might prevent accessing its internal structure [6]. This gives the advantage to other methods, like plunge freezing, where cryo-fixation of thick samples can be performed without the use of fillers. However, investigating large regions of plunge frozen samples with cryo-SEM can be limited, as it is difficult to obtain a suitable depth of vitrified ice in these samples. Verifying the depth of vitreous ice in plunge frozen samples has been reported to be a crucial step for accurate structural analysis with cryo-SEM [6].

Even though many authors demonstrated the possibility of identifying ice crystals by cryo-SEM imaging [12,13], a trained eye and a long experience in cryo-observation of hydrated materials are required for such a task. Also, distinguishing between vitreous and crystalline ice with cryo-SEM is generally based on their difference in terms of contrast [14] or geometry [12]. The error rate of making a statement about the vitreous state of water without the presence of ice crystals around, or near the region of analysis, can be very large. It is therefore important to resort to other characterization tools better suited for examining the crystalline/amorphous structure of aqueous phases in order to

avoid uncertainties associated with mere visual inspections. Electron and X-ray diffraction techniques are quite adapted to reveal the material crystalline structure and were used in multiple studies to detect crystalline ice in frozen samples [15-19]. The limiting requirement of working with a well-defined geometry to perform electron diffraction (e.g. thin samples for transmission-electron diffraction and polished surfaces for electron backscattered diffraction) makes X-ray diffraction more suited for investigating thick non-polished materials. Nevertheless, the low flux of radiation in conventional X-ray diffraction can also be a limiting factor with regards to studying weak X-ray diffusing compounds such as ice [20]. The use of synchrotron radiation might be necessary in that case [19] but not many laboratories have the possibility or the financial requirements to have access to or host a synchrotron facility.

Numerous studies have reported the possibility of conducting Raman spectrometry to characterize hydrated and biological samples exhibiting irregular geometries [21-23]. The ability of this technique to identify crystalline and amorphous forms of ice at cryogenic temperatures has already been proven [24,25]. Given the spatial resolution (~ 1-10 µm) provided by µ-Raman spectrometry (µRaman) [26], ice crystals can be detected within a sub-picoliter volume. In addition, the development of correlative cryo SEM-µRaman [27, 28] has made it possible to analyze micro-sized sites in frozen hydrated sample using both techniques, which enables to perform *in situ* investigation and correlate between structural and chemical information obtained from the same regions of analysis. Despite the fact that these advantages make µRaman a robust tool to efficiently examine the state of ice in plunge frozen samples and at a micrometer cube volume of interest, methods for evaluating the depth of vitreous ice using correlative cryo SEM-µRaman are yet to be developed. Not only that such methods should provide a way to investigate the structure of ice at a precise depth but also to reduce fluorescence effects in µRaman [29]. In correlative SEM-µRaman, samples are usually coated with a metal conductive layer and resonance fluorescence from the metal should be minimized in order to obtain well-resolved Raman spectra.

In this work, we present a proof of principle study based on the use of a cryo focused ion beam (cryo-FIB)-SEM-µRaman instrument to evaluate cryo-fixation with plunge freezing *in-situ*. Milled trenches with a precise thickness can be obtained with FIB [30] which gives the possibility to investigate the state of ice with µRaman at a desired depth within a frozen sample. Analyses were performed on a calcium phosphate cement (CPC) (prepared by mixing α-Tricalcium phosphate with 2.5%wt $Na_2HPO_4$ aqueous solution - Liquid/Powder ratio of 0.35) mixed with 10.5%wt of gelatin solution. The mixture was aged in a salty water (0.9 %wt NaCl) for 72 hours and was later cryo-fixed by plunge freezing into liquid nitrogen slush. The frozen sample was mounted on a cryo-stage inside the SEM chamber. CPC-hydrogel (e.g. CPC-gelatin) composites are widely studied in biomedicine, notably for their application in bone regeneration [31,32]. Owing to the fact that they are high water content hybrid biomaterials, their structure can be significantly affected due to cryo-fixation artefacts. These biomaterials are therefore a typical sample of interest that could benefit from an evaluation of the cryo-fixation process prior to their analysis, and were used to assess the validity of our approach.

## MATERIALS AND METHODS

FIB milling and SEM imaging were performed using a Zeiss Crossbeam 550L instrument consisting of a Capella FIB column ($Ga^+$ ion beam) and a Gemini II field emission-SEM (FE-SEM) column. The dual FIB-SEM is coupled to an "InVia" Renishaw µRaman equipped with a 532 nm laser line. The system is based on an "on axis" configuration enabling to measure the Raman signal inside the SEM chamber and directly under the SEM pole piece [33]. In this "on axis" set up, a pierced parabolic mirror is positioned in the axis of the electron beam to allow the passage of electrons, which enables to carry out both SEM imaging and µRaman backscattered analysis on the same region of interest (ROI) in the sample. The possibility of performing a simultaneous SEM-Raman analysis and on the same region is extremely advantageous, not only for avoiding to relocate the ROI which might be time consuming, but also for keeping track of local phase changes that occur at low temperatures.

The FIB-SEM-µRaman instrument is attached to a Quorum PP3010 gas-cooled cryo preparation system and can operate under cryogenic conditions. The cryo system covers a cryo-preparation chamber attached to the microscope and a workstation that include a nitrogen freezing station. Sputter coating by a Pt layer was carried out on the sample surface inside the preparation chamber to ensure its electrical conductivity and reduce charging effects during SEM imaging. A simplified representation of the cryo FIB-SEM experimental set up is shown in figure 1,a. In order to evaluate the crystalline/vitreous form of ice as a function of depth within the frozen sample, a trapezoid trench with a depth of about 20 µm at the smaller base (figure 1,b) was made by FIB. FIB milling was performed at the coincidence point where the ion and electron beams intersect (i.e. working distance of 5.1 mm with the sample tilted at an angle of 54° from normal). Ion and electron energies were set to 30 and 2 keV, respectively, using a current of 15 nA for ions and 0.1 nA for electrons. With these conditions, the time of FIB milling was optimized and charging effects were avoided during SEM imaging. µRaman analyses were further carried out at a sample tilt of 0° (figure 1, c), using an incident laser power of 2 mW per 20 $\mu m^2$ and an acquisition time of 120 s.

## RESULTS AND DISCUSSION

A Raman spectrum of the frozen CPC-gelatin sample was first measured at 123 K inside the FIB trench (figure 2, a). In figure 2,b, we show a comparison between the obtained spectrum and that of hexagonal ice Ih [34], which is the most common crystalline structure that forms at low pressures [35]. The absence of sharp peaks in the low frequency range (170 $cm^{-1}$- 330 $cm^{-1}$) suggests that the Raman signal does not correspond to that of Ih or to any of the known crystalline structures of ice [35]. It is most likely associated to an amorphous structure [24,34]. The spectrum does not however resemble to that of low density amorphous (LDA) ice that is expected to form at low pressures [24] but the similarity between the observed spectrum and that of super-cooled liquid water [24] suggests that the aqueous phase exhibits a disordered liquid-like structure.

The Raman spectrum of the CPC-gelatin mixture was also measured after warming the sample *in situ* by setting the cryo-stage at a T=153 K. By comparing measurements at 123 K and at 153 K, we were able to verify the sensitivity of µRaman to

the changes of the molecular arrangement of the aqueous solution when heated above the Tg water. As shown in figure 2,b, a difference can be observed, in the low frequency range, between the Raman spectra measured at the two working temperatures. A sharp peak was observed at ~199 $cm^{-1}$ in the spectrum acquired at 153 K. The Raman band observed at ~199 $cm^{-1}$ is most likely associated with a translational lattice mode of a crystalline phase that was formed within the aqueous solution after heating [36]. Generally, warming vitreous ice to temperatures above 143 K results in an irreversible transformation of the amorphous structure to Ih [37]. In our case, the translational mode is observed at a lower frequency than that in Ih (212 $cm^{-1}$- 220 $cm^{-1}$) [35,38-40]. It is therefore not certain that this band comes from Ih crystals that are expected to form at 153 K. We believe that this might be related to the presence, even weak, of NaCl in the aqueous phase. Hydrohalite ($NaCl\text{-}2H_2O$) crystals were shown to be easily identified with Raman in solutions with very low NaCl content [41]. In these crystals, translational modes can occur at a frequency lower than that in Ih. *R.W. Berg* identified the presence of this mode at ~192 $cm^{-1}$ in Raman spectrum of hexagon hydrohalite crystal measured at 253 K [36]. The upshift in the frequency (199 $cm^{-1}$ instead of 192 $cm^{-1}$) can be explained by the fact that measurements in our study were performed at a lower temperature than in Berg's study. The frequencies of transitional modes in aqueous phases are very dependent of the temperature [34,39] due to the effects of anharmonicity on intermolecular vibrations [42]. A decrease of the temperature leads to an increase in the frequency of translational vibrations in anharmonic crystals [42].

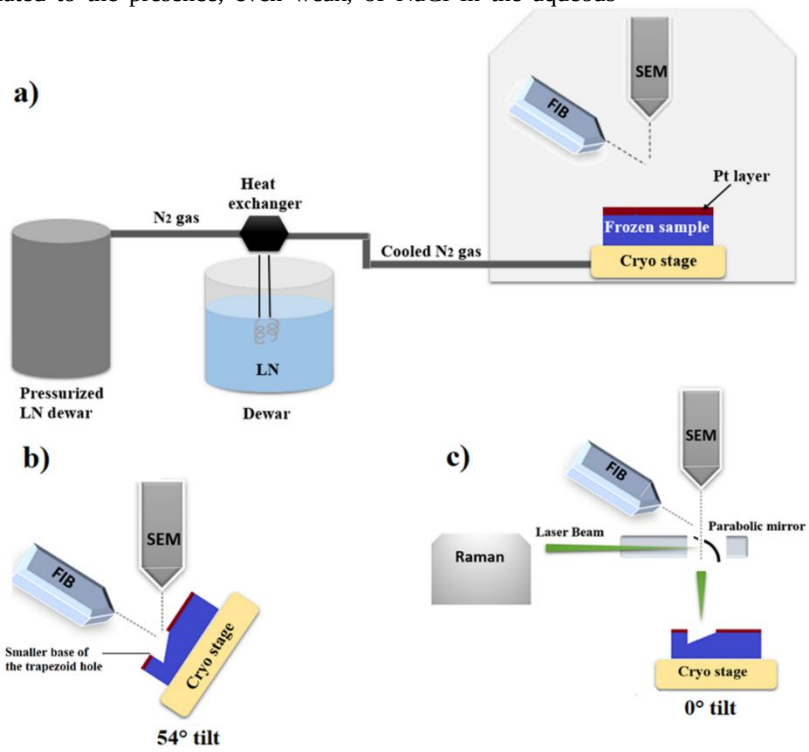


Figure 1. a) Set up for the FIB-SEM experiments under cryogenic conditions. b) FIB milling of a trench within the frozen sample and c) the "on axis" SEM-µRaman set up with the positioning of a parabolic mirror pierced to allow the passage of the electron beam for SEM imaging and to carry out µRaman backscattered analysis inside the trench.

A simple explanation of the different transitions that occurred at the zone of analyses is suggested in figure 2,c. The aqueous phase most likely went from a liquid to an amorphous state upon rapid cooling by plunge freezing into liquid nitrogen slush and, when heated up to 153 K, hexagon hydrohalite crystals were formed inside the amorphous phase. A similar phenomenon, although not very common, was observed in cryo-preserved biological samples, where only a growth of hydrohalite crystals within frozen cells was detected without the formation of crystalline ice [43]. In our case, this can be partly related to the presence of gelatin, as it was reported that the high viscosity of aqueous gelatin solutions and the constrained spatial distribution of water prevent ice crystallites from growing [44].

Verifying if the band at 199 $cm^{-1}$ really comes from a crystalline hydrohalite would require to heat the sample up to 253 K and evaluate the frequency shift due to the variation of the temperature. However, because all our experiments were carried out under vacuum inside the SEM chamber, dehydration of the sample due to ice sublimation started to appear when the cryo-stage was heated above 175 K-180 K (total dehydration occurred at 193 K as shown in figure 3). In order to avoid ice sublimation, the temperature dependence of the translational mode was instead studied at a lower temperature. The sample was cooled back to 123 K and the Raman spectrum measured after re-cooling the sample was compared the one measured at 153 K. As shown in figure 4, the Raman band at ~199 $cm^{-1}$ is also detected at 123 K but appears to be upshifted by 1 $cm^{-1}$ when decreasing the temperature. This indicates that the mode is indeed dependent on the temperature and shifts to higher frequencies when the temperature increases.

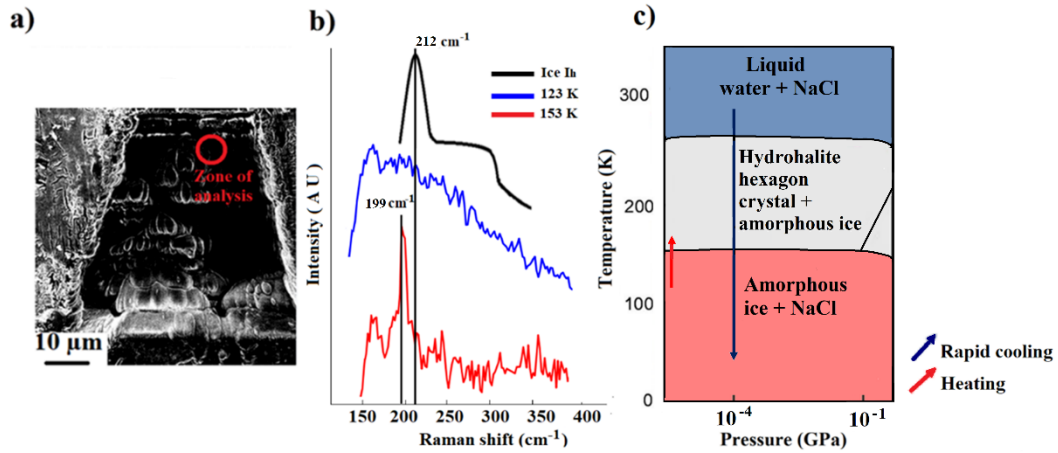


Figure 2 a) Cryo SEM micrograph showing the trapezoid hole made by FIB and the zone of µRaman analysis. b) µRaman spectra measured at two different temperatures 123 K and 153 K and a comparison between the two spectra and that of hexagonal ice Ih [34]. c) A simple representation of the possible transitions of the aqueous phase due to rapid cooling of the sample below the Tg of water and heating it up to 153 K.

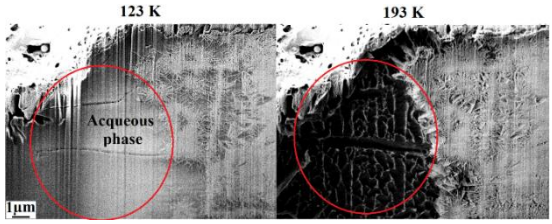


Figure 3. SEM micrographs showing the face of the trapezoid trench at a sample tilt of 54°. The comparison between the images acquired at 123 K and 193 K shows that a complete dehydration of CPC/gelatin has occurred at 193 K due to ice sublimation.

### Advantages of FIB in reducing fluorescence emission in µRaman spectra

The results presented in this section highlight the benefits of using FIB for reducing fluorescence effects in metal coated samples and improving the results obtained with correlative SEM-µRaman. Analyses with µRaman were performed on different ROIs of the frozen CPC-gelatin sample (zones 1, 2 and 3 in figure 5) at 123 K. The results clearly show that Raman signal is significantly affected by fluorescence effects when analysis is performed at the sample surface (zone 1), whereas an improved signal was obtained inside the trapezoid trench (zone 3). The Raman spectrum associated with zone 2 indicates that probing the sample at a region of the trench close to the surface also results in a remaining intense fluorescence background [29].

The absorption of the excitation laser by the Pt coating layer results in the emission of a continuous fluorescence signal. Although conductive coating is important for reducing charging effects in SEM, it can significantly affect µRaman results. Removing the metal layer from the micro-sized region of analysis using FIB can therefore be a practical solution for reducing fluorescence, while maintaining an electrical conductivity in the rest of the sample for SEM observations.

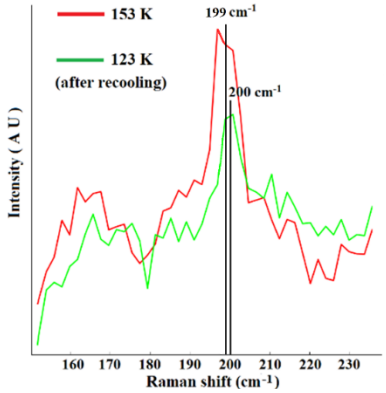


Figure 4. A comparison of Raman spectrum measured at 153 K and the one acquired after cooling the sample back to 123 K.

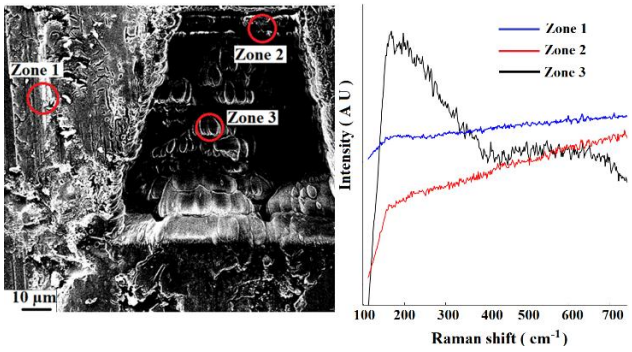


Figure 5. Cryo SEM micrograph of a frozen CPC-gelatin mixture at 123 K showing the trapezoid trench made by FIB and the zones of µRaman analyses (left). The corresponding µRaman analyses performed under cryogenic conditions on each zone (right).

## CONCLUSION

Analysis with a FIB-SEM-µRaman instrument operating under cryogenic conditions was achieved for the first time, and showed the substantial potential of this instrument with regards to evaluating the accuracy of cryo-fixation by plunge freezing. With FIB enabling to mill the sample with a defined thickness, low frequency µRaman can be applied to examine

the state of water at a given depth within a frozen sample. µRaman enabled to identify a vitreous aqueous phase at a depth of about 20 µm in a plunge frozen CPC/gelatin compound that was embedded in an $NaCl/H_2O$ solution. Upon warming the sample up to 153 K, hydrohalite crystals were detected locally at the region of analysis with µRaman. Not only that FIB milling allowed for µRaman characterizations in depth, but was also practical for removing the conductive layer at a specific region and thereby reducing fluorescence effects. The use of FIB can therefore be necessary to minimize the fluorescence parasitic background and obtain resolved Raman spectra. Overall, such a methodology should provide very useful elements for studies of complex biological tissues containing saline solutions.

We note that for FIB milling, the angle of incidence should be low to minimize the deposition effect of milled material during the milling process. In fact, in FIB-SEM experiments, FIB milling is typically done along the surface of the support. Besides wedge-shaped milling, more sophisticated strategies (e.g. cryo-lamellas) could be envisioned in the future in order to ensure parallel milling of the studied surface and avoid possible ion deposition effects. Although interactions of $Ga^+$ ions with frozen hydrated samples was considered in a previous study and showed that FIB milling did not cause their devitification [45], finding suitable conditions for milling might be essential in the case of beam sensitive samples to avoid altering their composition.

## AUTHOR INFORMATION

### Corresponding Authors

*__Mouad Essani__ - Nantes Université, CNRS, Institut des Matériaux Jean Rouxel de Nantes (IMN), F-44000 Nantes, France
*__Patricia Abellan__ - Nantes Université, CNRS, Institut des Matériaux Jean Rouxel de Nantes (IMN), F-44000 Nantes, France

### Notes

The authors declare no competing financial interest.

## ACKNOWLEDGMENT

PA and ME would like to thank the financial support provided by the NExT initiative through the French National Research Agency (ANR) under the Programme d'Investissements d'Avenir (with reference ANR-16-IDEX-0007). The e-BRIDGE project also receives financial support from the Pays de la Loire region and Nantes Métropole. FIB/SEM data were collected in the CIMEN Electron Microscopy Center in Nantes, funded by the French Contrat Plan État-Région and the European Regional Development Fund of Pays de la Loire.

## REFERENCES

(1) Zachman, M. J.; Tu, Z.; Choudhury, S.; Archer, L. A.; Kourkoutis, L. F. Nature 2018, 560 (7718), 345–349.
(2) Zachman, M. J.; de Jonge, N.; Fischer, R.; Jungjohann, K. L.; Perea, D. E. MRS Bull. 2019, 44 (12), 949–955.
(3) DeRocher, K. A.; Smeets, P. J. M.; Goodge, B. H.; Zachman, M. J.; Balachandran, P. V.; Stegbauer, L.; Cohen, M. J.; Gordon, L. M.; Rondinelli, J. M.; Kourkoutis, L. F.; Joester, D. Nature 2020, 583 (7814), 66–71.
(4) Che, R.; Gu, D.; Shi, L.; Zhao, D. J. Mater. Chem. 2011, 21 (43), 17371.
(5) Hoch, H. C.; Mendgen, K., Lesemann, D.-E., Eds.; Springer Berlin Heidelberg: Berlin, Heidelberg, 1991; pp 1–16.
(6) Aston, R.; Sewell, K.; Klein, T.; Lawrie, G.; Grøndahl, L. European Polymer Journal 2016, 82, 1–15.
(7) Sitte, H.; Edelmann, L.; Neumann, K. In Cryotechniques in Biological Electron Microscopy; Steinbrecht, R. A., Zierold, K., Eds.; Springer Berlin Heidelberg: Berlin, Heidelberg, 1987; pp 87–113.
(8) Moor, H.; Steinbrecht, R.A.; Zierold, Z.; (Eds.). Springer-Verlag, Berlin (1987), pp. 175-19
(9) https://www.sciencedirect.com/topics/biochemistry-genetics-and-molecular-biology/cryoprotectant
(10) McDonald, K. L.; Morphew, M.; Verkade, P.; Müller-Reichert, T.; Kuo, J., Ed.; Walker, J. M., Series Ed.; Methods in Molecular Biology; Humana Press: Totowa, NJ, 2007; Vol. 369, pp 143–173.
(11) Serp, D.; Mueller, M.; von Stockar, U.; Marison, I. W.; Biotechnol. Bioeng. 2002, 79 (3), 253–259.
(12) Gosden, R. G.; Yin, H.; Bodine, R. J.; Morris, G. J. Character.; Human Reproduction 2010, 25 (2), 470–478.
(13) McCULLY, M. E.; Canny, M. J.; Huang, C. X.; Annals of Botany 2004, 94 (5), 665–674.
(14) de Winter, D. A. M.; Mesman, R. J.; Hayles, M. F.; Schneijdenberg, C. T. W. M.; Mathisen, C.; Post, J. A. Journal of Structural Biology 2013, 183 (1), 11–18.
(15) Courtas, S.; Grégoire, M.; Federspiel, X.; Bicaïs-Lepinay, N.; Wyon, C. Microelectronics Reliability 2006, 46 (9–11), 1530–1535.
(16) Majewski, J.; Margulis, L.; Jacquemain, D.; Leveiller, F.; Bohm, C.; Arad, T.; Talmon, Y.; Lahav, M.; Leiserowitz, L. Science 1993, 261 (5123), 899–902.
(17) McDowall, A. W.; Chang, J.-J.; Freeman, R.; Lepault, J.; Walter, C. A.; Dubochet, J. Journal of Microscopy 1983, 131 (1), 1–9.
(18) Berejnov, V.; Husseini, N. S.; Alsaied, O. A.; Thorne, R. E. Effects of Cryoprotectant Concentration and Cooling Rate on Vitrification of Aqueous Solutions. J Appl Crystallogr 2006, 39 (2), 244–251.
(19) Anzar, M.; Grochulski, P.; Bonnet, B. PLoS ONE 2014, 9 (12), e114801.
(20) Chen, J.-Y.; Kim, M.; Yoo, C.-S.; Liermann, H.-P.; Evans, W. J. J. Phys.: Conf. Ser. 2014, 500 (14), 142006.
(21) Stone, N.; Baker, R.; Rogers, K.; Parker, A. W.; Matousek, P. Analyst 2007, 132 (9), 899.
(22) Huang, Z.; McWilliams, A.; Lui, H.; McLean, D. I.; Lam, S.; Zeng, H. Int. J. Cancer 2003, 107 (6), 1047–1052.
(23) Butler, H.; Ashton, L.; Bird, B; et al. Nat Protoc 2016, 11, 664–687.
(24) Suzuki, Y.; Takasaki, Y.; Tominaga, Y.; Mishima, O. Chemical Physics Letters 2000, 319 (1–2), 81–84.
(25) Suzuki, Y.; Mishima, O. The Journal of Chemical Physics 2002, 117 (4), 1673–1676.
(26) Potgieter-Vermaak, S. S.; Van Grieken, R. Appl Spectrosc 2006, 60 (1), 39–47.
(27) Hazekamp, J.; Reed, M. G.; Howard, C. V.; Van Apeldoorn, A. A.; Otto, C. Journal of Microscopy 2011, 244 (2), 122–128.
(28) Lopez-Sanchez, P.; Schumm, S.; Pudney, P. D. A.; Hazekamp, J. Analyst 2011, 136 (18), 3694.
(29) Panczer G, De Ligny D, Mendoza C, Gaft M, Sexdoux-Guillaume A, Wang X (2012) Raman and fluorescence. In: Dubessy J, Caumon M-C, Rull F (eds). Eur Mineral Union Notes in Mineralogy, vol 12. Eur Mineral Union and Mineral Soc of Great Britain and Ireland, pp 61–82
(30) Giannuzzi, L. A.; Stevie, F. A. Micron 1999, 30 (3), 197–204.
(31) Xu, H. H.; Wang, P.; Wang, L.; Bao, C.; Chen, Q.; Weir, M. D.; Chow, L. C.; Zhao, L.; Zhou, X.; Reynolds, M. A. Bone Res 2017, 5 (1), 17056.
(32) Kovtun, A.; Goeckelmann, M. J.; Niclas, A. A.; Montufar, E. B.; Ginebra, M.-P.; Planell, J. A.; Santin, M.; Ignatius, A. Acta Biomaterialia 2015, 12, 242–249.
(33) Schmidt, R.; Fitzek, H.; Nachtnebel, M.; Mayrhofer, C.; Schroettner, H.; Zankel, A. Macromol. Symp. 2019, 384 (1), 1800237.
(34) Furić, K.; Volovšek, V. J. Mol. Struct. 2010, 976 (1–3), 174–180.
(35) Minceva-Sukarova, B.; Sherman, W. F.; Wilkinson, G. R. J. Phys. C: Solid State Phys. 1984, 17 (32), 5833–5850.
(36) Berg, R. W. Applied Spectroscopy Reviews 2018, 53 (6), 503–515.
(37) Dowell, L. G.; Rinfret, A. P. Nature 1960, 188 (4757), 1144–1148.
(38) Ockman, N. Advances in Physics 1958, 7 (26), 199–220.
(39) Krishnamurthy, S.; Bansil, R.; Wiafe- Akenten, J. The Journal of Chemical Physics 1983, 79 (12), 5863–5870.
(40) Wong, P. T. T.; Whalley, E. J. Chem. Phys. 1976, 65 (2), 829–836.
(41) Dubessy, J.; Audeoud, D.; Wilkins, R.; Kosztolanyi, C. Chem. Geol. 1982, 37 (1–2), 137–150.
(42) Johari, G. P.; Chew, H. A. M. Philosophical Magazine B 1984, 49 (3), 281–294.
(43) Kreiner-Møller, A.; Stracke, F.; Zimmermann, H. Hydrohalite. Cryobiology 2014, 69 (1), 41–47.

(44) Dowell, L. G.; Moline, S. W.; Rinfret, A. P. Biochim Biophys Acta 1962, 59 (1), 158–167.
(45) Marko, M.; Hsieh, C.; Moberlychan, W.; Mannella, C. A.; Frank, J. J Microsc 2006, 222 (1), 42–47.

TOC